


 Cite this: *Soft Matter*, 2020, 16, 9890

Surface charge density and fatty acids enhance the membrane permeation rate of CPP–cargo complexes

 Matías A. Via, ^a Natalia Wilke,^{bc} Luis S. Mayorga^{ad} and Mario G. Del Pópolo ^{*ae}

The CPP-effect makes reference to the process by which the membrane translocation rate of a cargo is enhanced by chemical functionalization with cell-penetrating peptides (CPPs). In this work we combine a simple kinetic model with free-energy calculations to explore the energetic basis of the CPP-effect. Two polyglycines are selected as model hydrophilic cargoes, and nona-arginine as a prototypical CPP. We assess the cargo carrying efficiency of nona-arginine by comparing the adsorption and insertion energies of the cargoes, the cargo-free CPPs, and the CPP–cargo complexes, into lipid membranes of varying composition. We also analyze the effect of modifying the type and concentration of anionic lipids, and the implication of these factors on the translocation rate of the CPP–cargo complex. Of particular interest is the evaluation of the catalytic role of palmitic acid (palmitate) as a promoter of the CPP-effect. We also analyse the influence of the size of the cargo on the membrane adsorption and insertion energies. Our results show that the efficiency of nona-arginine as a transmembrane carrier of simple hydrophilic molecules is modulated by the size of the cargo, and is strongly enhanced by increasing the concentration of anionic lipids and of ionized fatty acids in the membrane.

 Received 15th April 2020,
Accepted 22nd September 2020

DOI: 10.1039/d0sm00673d

rsc.li/soft-matter-journal

1 Introduction

Cell-penetrating peptides (CPPs), also known as trojan peptides, are recognized by their remarkable capacity to translocate lipid membranes.^{1,2} These highly-charged hydrophilic molecules are suitable as vectors for intracellular drug delivery, as they confer membrane permeation properties to otherwise membrane-impermeable “cargoes”, such as macromolecules (proteins, DNA and RNA strands)^{3–6} and bioimaging agents (fluorophores and quantum dots).^{7–10} Increasing a cargo’s permeation rate *via* functionalization with cell-penetrating peptides is known as the “CPP-effect”. Currently, there is much need to understand how the CPP–cargo complexes traverse lipid bilayers, and to identify the physicochemical variables that most effectively regulate the CPP-effect.^{11–14}

The cellular intake of a CPP–cargo complex may occur by endocytosis, by direct translocation of the cell membrane, or through a combination of these two mechanisms.^{15–19} However, in all cases, the complex must eventually diffuse across a lipid bilayer in order to reach the cytoplasm. Either the complex translocates the plasma membrane, or it must physically cross the endosomal membranes whenever the uptake follows the endocytic pathway.

Several permeation mechanisms have been proposed for cargo-free CPP molecules,^{18,20–25} being the opening of hydrophilic transmembrane pores a common ingredient among most models.^{26–30} The exact physical pathways that CPPs follow when moving across a lipid bilayer depend both on the sequence of the peptide and the chemical composition of the membrane,^{18,31} and there is growing consensus that pre-concentration, or peptides’ adsorption on the membrane surface, plays a critical role during the initial stages of permeation.³²

However, when it comes to CPPs chemically bound to a cargo, much less is known about the energetics and the configurational changes that take place when the CPP–cargo complex moves across the membrane. In the most general terms, and in line with the cationic identity of CPPs, the membrane translocation mechanism involves the following stages: (1) diffusion and adsorption of the complex on the negatively charged surface of the cell; (2) transit of the CPP–cargo complex across the membrane, with the concomitant formation of a transient structure, or transition state; (3) release of

^a Facultad de Ciencias Exactas y Naturales, Universidad Nacional de Cuyo, Mendoza, CP5500, Argentina. E-mail: mdelpopolo@fcen.uncu.edu.ar

^b Centro de Investigaciones en Química Biológica de Córdoba (CIQUIBIC-CONICET), Argentina

^c Departamento de Química Biológica Ranwel Caputto, Facultad de Ciencias Químicas, Universidad Nacional de Córdoba, Córdoba X5000HUA, Argentina

^d Instituto de Histología y Embriología de Mendoza (IHEM) CONICET-UNCUYO, Mendoza, CP5500, Argentina

^e Instituto Interdisciplinario de Ciencias Básicas (ICB), CONICET-UNCUYO, Mendoza, CP5500, Argentina. E-mail: mdelpopolo@mendoza-conicet.gob.ar

the complex from the inner leaflet of the cell membrane. The whole process occurs under kinetic control, and the characteristic time of each stage can in principle be modulated by the chemical properties of the CPP, the size and shape of the cargo,¹⁹ the CPP density on the surface of the cargo, the chemical composition of the membrane,²⁷ the interfacial electric field,³⁰ and the concentration of CPP–cargo complexes in the extra-cellular medium.

Significant efforts have been dedicated to the calculation of translocation free-energy profiles for cargo-free CPP molecules, to the careful examination of translocation mechanisms, and to uncover the impact of physicochemical parameters, such as membrane and peptide composition, on the energetic of peptides' adsorption and insertion into the membrane.^{27,30,33,34} However, when it comes to CPP-functionalized cargoes, the thermodynamic assessment of transport mechanisms by means of molecular simulations are much more scarce. In one of the few simulation studies available, Lin *et al.* have shown that a nanoparticle decorated with the HIV-1 Tat peptide can spontaneously cross a lipid bilayer under the driving force of an intense electric field.³⁵ The crossing of the membrane involves the opening of a transmembrane pore that closes when the nanoparticle reaches the distal side of the membrane. Also, Li *et al.* have evaluated translocation free-energy profiles for hydrophobic and hydrophilic particles decorated with polyarginines.³⁶ These authors considered bilayers with an asymmetric distribution of anionic lipids between leaflets, which produces an electric field that pushes the particles across the membrane.

The present work aims at characterizing how a prototypical cell-penetrating peptide (nona-arginine, R₉) modulates the translocation of simple hydrophilic cargoes (polyglycines), across lipid bilayers. With this purpose, we will first consider a simple phenomenological model that highlights the relevant kinetic and thermodynamic parameters controlling membrane translocation. Within the conceptual framework of that model we will then perform coarse-grained molecular dynamics simulations to compute translocation free-energy profiles for a single CPP molecule, a single cargo molecule, and the corresponding CPP–cargo complex. As stated before, as a prototypical CPP we will resort to R₉, and as a first hydrophilic cargo we will consider nona-glycine, G₉. The comparison of free-energy profiles between the CPP and the CPP–cargo complex (R₉G₉) will shed light on the kinetic basis of the CPP-effect.

Secondly, we will assess the role of the surface charge and the chemical composition of the membrane on the effectiveness of the CPP-effect. With this aim, we will compute adsorption and insertion free-energies for R₉ and R₉-cargo complexes into binary membranes made of DOPC (dioleoylphosphatidylcholine) and varying amounts of the anionic lipid DOPG (dioleoylphosphatidylglycerol). In order to separate surface charge and chemical composition effects, we will also consider membranes where the negative charge is provided by deprotonated palmitic acid (PA⁻). DOPG and PA⁻ bear the same negative charge but differ in molecular size, shape and mobility. Also, PA⁻ has been shown to enhance the insertion and transport of cargo-free polyarginines across lipid membranes.^{33,37}

Finally, we will address how the size of the hydrophilic cargo influences the efficiency of R₉ as a CPP. This will be done by

comparing the translocation free-energies of R₉G₉ and R₉G₃₁, *i.e.* the CPP bound to linear polyglycines of different lengths.

On the whole, our results show that a typical CPP, like R₉, increases the translocation rate of the cargo by altering the balance between the cargo's binding energy to the membrane surface and the energy cost to jump across the bilayer. Recognizing the key role of adsorption and activation energies allows us to explain why, and to what extent, increasing the membrane's negative surface charge and its concentration of fatty acids enhances the CPP-effect. It also highlights the potential role of environmental factors, such as pH and salt concentration, as strong modulators of the CPP-effect.

2 Computational methods

Molecular Dynamics (MD) simulations were performed with the GROMACS-5.1.2 code.³⁸ The interactions between the components of the system were computed according to the polarizable MARTINI coarse-grained force field.³⁹ All systems consisted of a membrane patch of 336 lipids oriented perpendicular to the *z*-axis of an orthorhombic simulation box. Initial configurations were generated with the *Insane* program,⁴⁰ and minimized using the steepest descent method. Each system was first equilibrated for 10 ns in the *NVT* ensemble, followed by other 10 ns under isotropic *NPT* conditions. The final average dimensions of the simulation box were 10.9 × 10.9 × 22.5 nm. The membrane was solvated with ~20 000 water molecules. A single peptide molecule was placed in the bulk solution, together with its corresponding counterions in order to maintain electroneutrality. As stated before, we choose nona-arginine (R₉) as a representative CPP, and two linear polyglycines (pGly), G₉ and G₃₁, as cargoes. Both G₉ and G₃₁ are water soluble and have no cell-permeation properties.

In all cases the integration time step was 20 fs and the neighbours list was updated every 10 MD steps. The temperature and pressure conditions of the simulations were 310 K and 1 bar, respectively, which were maintained using the Berendsen thermostat (time constant $t_T = 0.3$ ps) and the semi-isotropic Berendsen barostat (time constant $t_P = 3.0$ ps, and a compressibility of 3.0×10^4 bar⁻¹). Non-bonded interactions were cutoff at 1.2 nm and switched smoothly to zero from 0.9 nm. Electrostatic forces were computed using the particle mesh Ewald method (3d geometry), with a real space cut-off of 1.2 nm and a Fourier spacing of 0.2 nm.

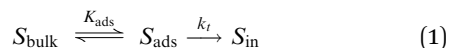
Free-energy profiles were computed by Umbrella Sampling (US).⁴¹ The reaction coordinate, or order parameter, was the *z*-component of the distance vector between the center of mass (COM) of the peptide and the COM of the lipid bilayer. In all cases the reaction coordinate was sampled using harmonic restraining potentials. Between the centre and the surface of the membrane, US windows were placed every 0.1 nm (force constant of 5000 kJ mol⁻¹). Within the aqueous solution they were placed every 0.4 nm (force constant of 300 kJ mol⁻¹). Each US window was equilibrated for 100 ns and production runs were extended for another 300 ns. Free-energy profiles were recovered by using the weighted histogram analysis method (WHAM).⁴²

A summary of the 13 systems simulated in this work is provided below. We specify the peptide and the bilayer composition, where %PG represents the percentage of DOPG in the DOPC–DOPG bilayer, and %PA(H) the corresponding ionized (PA) or protonated (PAH) palmitic acid in the PA(H)–DOPC bilayer: (1) R₉-0%PG; (2) R₉-10%PG; (3) R₉-30%PG; (4) R₉-50%PG; (5) R₉-25%PA; (6) R₉-25%PAH; (7) R₉G₉-0%PG; (8) R₉G₉-30%PG; (9) R₉G₉-50%PG; (10) R₉G₉-25%PA; (11) G₉-50%PG; (12) R₉G₃₁-30%PG; (13) G₃₁-30%PG.

3 Results

Consider the case of a cargo and of a cell-penetrating peptide that traverse a lipid membrane at rates v^{cargo} and v^{CPP} , respectively. Functionalization of the cargo with certain number of CPP molecules produces a CPP–cargo complex that traverses the membrane at a rate $v^{\text{CPP-cargo}}$. We are interested in the case where the CPPs accelerate the passive transport of the cargo, so that $v^{\text{CPP-cargo}} > v^{\text{cargo}}$. The efficiency of the CPP-effect can be quantified by the relative translocation rate $w = v^{\text{CPP-cargo}}/v^{\text{cargo}}$. For all practical purposes, w must be greater than one, although its actual value will depend on a series of factors, such as the cargo's size and shape, the number of functionalizing CPP molecules, the chemical composition of each of the membrane leaflets, the pH and salt concentration gradient across the membrane, the transmembrane potential, *etc.*

For any of the chemical species, S , considered in the previous paragraph ($S = \text{CPP}$, cargo, or CPP–cargo complex) the rate of passive transport across the membrane is determined by the combined efficiency of the following processes:



Species S approaches the “outer” leaflet of the membrane from a bulk solution of concentration $[S]^{\text{bulk}}$. For simplicity, we consider that the “inner” leaflet of the membrane is in contact with a solution where $[S]^{\text{bulk}} = 0$ (intracellular space). The first two processes in eqn (1) correspond to the adsorption/desorption of S on/from the membrane surface, which we consider to be in dynamical equilibrium and characterized by the equilibrium constant $K_{\text{ads}} = [S]_{\text{eq}}^{\text{ads}}/[S]_{\text{eq}}^{\text{bulk}} = e^{-\beta\Delta G_{\text{ads}}}$, where $[S]_{\text{eq}}^{\text{ads}}$ and $[S]_{\text{eq}}^{\text{bulk}}$ are the equilibrium concentrations of S on the surface of the membrane and in the bulk, respectively, and ΔG_{ads} is the adsorption free-energy.

The third stage of the mechanism corresponds to the thermally activated jump of S across the bilayer, occurring at a rate $v = k_t[S]_{\text{eq}}^{\text{ads}}$, with k_t given by Arrhenius equation $k_t = \alpha e^{-\beta\Delta G_{\text{act}}}$. In this equation α is a pre-exponential factor and ΔG_{act} is the free-energy cost to create the transition state, *i.e.* the configuration that introduces a kinetic bottleneck in the process. Fig. 1 shows a schematic free-energy profile for the translocation of S across a lipid membrane. As in the simulations discussed below, the reaction coordinate, z , represents the distance between the centre of mass of the membrane and the centre of mass of the approaching object. ΔG_{ads} , ΔG_{act} , and $\Delta G_{\text{ins}} = \Delta G_{\text{ads}} + \Delta G_{\text{act}}$ are marked on the graph. This latter quantity, in particular, represents the cost to bring S from the bulk solution to the configuration of the transition state.

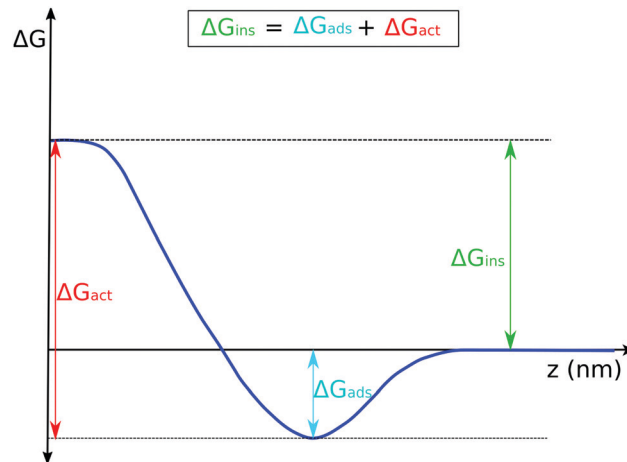


Fig. 1 Schematic free-energy profile associated to the membrane translocation by any of the species, S , considered in the text ($S = \text{CPP}$, cargo, or CPP–cargo complex). z represents the distance between the centre of mass of the membrane and the centre of mass of the approaching object. ΔG_{ads} and ΔG_{act} are the free-energy costs associated to the adsorption of S on the membrane surface, and the formation of the transition state (activation barrier), respectively. $\Delta G_{\text{ins}} = \Delta G_{\text{ads}} + \Delta G_{\text{act}}$ represents the cost to bring S from the bulk solution to the configuration of the transition state.

Putting the previous equations together, the translocation rate of S can be written as:

$$v^S = \alpha^S [S]_{\text{eq}}^{\text{bulk}} e^{-\beta\Delta G_{\text{ins}}^S} \quad (2)$$

which shows that the flux of S across the membrane is mostly determined by the competition between the adsorption energy and the energy penalty for creating the transition state.^{32,43} Also, notice that under similar concentrations of species S_a and S_b in the bulk, and assuming that $\alpha^{S_a} \sim \alpha^{S_b}$, the relative translocation rate of S_b with respect to S_a is,

$$w = \frac{v_b}{v_a} \sim e^{\beta(\Delta G_{\text{ins}}^{S_a} - \Delta G_{\text{ins}}^{S_b})} \quad (3)$$

3.1 R₉ confers membrane permeation properties to the non-permeable peptide G₉

Polyarginines have proven to be effective carriers of multiple cargoes such as peptides, proteins, DNA molecules, and nanoparticles, amongst others. Furthermore, it has been shown experimentally that R₉ is one of the most efficient cell-penetrating peptides,^{44–48} and its permeation mechanism has been investigated by coarse-grained molecular dynamics simulations, as the ones used here,^{26,36,49} and other theoretical methods.^{28,32} At physiological pH, R₉ has a formal charge of +9. As starting point of our analysis, we calculated the free-energy cost to bring a single R₉ molecule from solution up to the centre of a DOPC/DOPG 1 : 1 bilayer. The same calculation was performed for our model hydrophilic cargo, the peptide G₉, which is electroneutral and is known to be a non-CPP sequence.

Fig. 2 shows the resulting free-energy profiles. For G₉, the free-energy (green curve) increases monotonically as the peptide goes into the membrane, indicating that the peptide prefers to

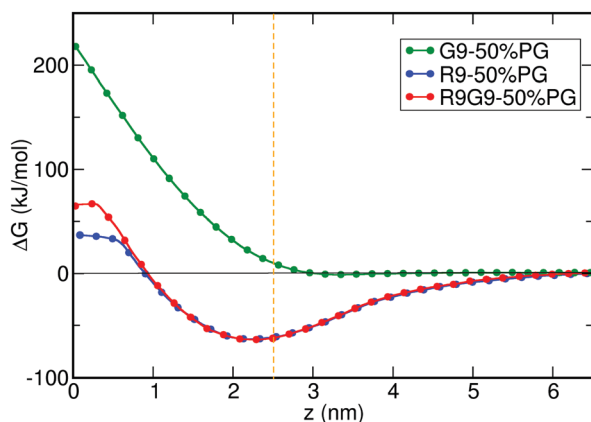


Fig. 2 Free-energy profiles for the translocation of R_9 (blue), G_9 (green) and the R_9G_9 complex (red) through a DOPC/DOPG 1:1 bilayer. The vertical dashed line indicates the average position of the membrane surface.

reside in solution, and that insertion into the membrane has a very high energy penalty ($\Delta G_{\text{act}}^{G_9} = 220 \text{ kJ mol}^{-1}$). In contrast, and as expected from previous publications,^{26,27} the free-energy profile of R_9 (blue curve) goes through a deep minimum and then rises abruptly as z approaches zero. The minimum corresponds to the most stable thermodynamic state of the CPP, when it is adsorbed on the negatively charged surface of the membrane ($\Delta G_{\text{ads}}^{R_9} = -61 \text{ kJ mol}^{-1}$). The maximum corresponds to the transition state, when the peptide reaches the center of the membrane ($\Delta G_{\text{ins}}^{R_9} = 98 \text{ kJ mol}^{-1}$). The resulting insertion energies for G_9 and R_9 are ($\Delta G_{\text{act}}^{G_9} = 220 \text{ kJ mol}^{-1}$) and ($\Delta G_{\text{ins}}^{R_9} = 37 \text{ kJ mol}^{-1}$), respectively, which according to eqn (3) indicate that R_9 is expected to cross the membrane 30 orders of magnitude faster than G_9 . In a laboratory experiment this is equivalent to say that R_9 permeates the membrane while G_9 does not.

Still, in order to quantify the carrier capacity of R_9 , we chemically coupled the two peptides and calculated the translocation free-energy profile for the CPP-cargo complex R_9G_9 . From the red and blue profiles of Fig. 2 one can see that the values of ΔG_{ads} for R_9 and R_9G_9 are quite similar. This is readily explained by the fact that G_9 has no net electrical charge, so that the binding of R_9G_9 to the membrane surface is entirely driven by the polyarginine sequence. At the same time, when comparing the insertion free-energies of the naked and functionalized cargoes, $\Delta G_{\text{ins}}^{G_9} = 220 \text{ kJ mol}^{-1}$ and $\Delta G_{\text{ins}}^{R_9G_9} = 60 \text{ kJ mol}^{-1}$, it becomes clear why the CPP sequence confers membrane permeation ability to G_9 . The ΔG_{ins} of G_9 decreases by a factor of 3.6 when adding 9 arginine residues, which results in a 26 orders of magnitude increase in translocation rate, according to eqn (3). On the other hand, and as one may expect, the CPP-cargo complex translocates the membrane 7500-times slower than the cargo-free CPP molecule.

For the particular systems under consideration, our simulations indicate that the CPP-effect stems both from a deeper adsorption

energy well, and a lower activation barrier for the CPP-cargo complex. The first factor induces the pre-concentration of the complex on the surface of the membrane ($\Delta G_{\text{ads}}^{G_9} = 0 \text{ kJ mol}^{-1}$, $\Delta G_{\text{ads}}^{R_9G_9} = -61 \text{ kJ mol}^{-1}$). The second one shows that even the jump across the membrane is facilitated by the presence of the CPP ($\Delta G_{\text{act}}^{G_9} = 220 \text{ kJ mol}^{-1}$, $\Delta G_{\text{act}}^{R_9G_9} = -121 \text{ kJ mol}^{-1}$). In other words, the membrane insertion of the neutral hydrophilic peptide G_9 incurs a very high energy cost. Functionalization of G_9 with R_9 lowers such a cost by increasing the adsorption energy and decreasing the translocation barrier. Altogether, introducing a CPP sequence results in a larger number of membrane crossing events per unit time.

The visual inspection of simulation snapshots suggests qualitative differences in the structure of the transition state configurations produced by the naked cargo, the CPP, and the CPP-cargo complex. As can be observed from Fig. 3a and b the insertion of R_9 and R_9G_9 into the membrane is accompanied by the formation of hydrophilic transmembrane pores. In the present context we define a hydrophilic pore as a conduit, or defect, that breaks the continuity of the membrane along the normal. Apart from the peptide, the pore contains water of hydration and its rim is covered by phospholipids' hydrophilic heads and it is enriched in negatively charged DOPG. These observations coincide with previous findings for R_9 and other CPPs.^{27,32,50} In the case of R_9G_9 , however, we observe that the cargo sequence, G_9 , tends to stick out of the membrane (orange spheres in Fig. 3b).

On the other hand, the insertion of G_9 into the membrane induces a large local deformation, perturbing the packing of the lipids, and creating a pocket where there is not water of hydration nor salt ions (Fig. 3c). In fact, the surface of the membrane locally bends towards the membrane mid-plane suggesting the deformation is mostly elastic.

The different structures of the transition states produced by the three peptides can also be assessed from the snapshots and from the charge density profiles of Fig. 4. Judging from panels (a) and (b) of Fig. 3 R_9 nucleates the hydrophilic pore when reaching the center of the membrane. This is evidenced by the presence of DOPG polar head-groups (green curve) spanning the whole membrane width. Comparatively, in panel (c), the

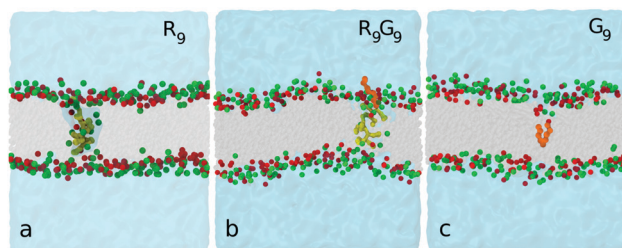


Fig. 3 Renderings of simulation snapshots when the peptides approach the centre of the membrane. (a) R_9 (yellow) and (b) R_9G_9 (R_9 in yellow and G_9 in orange) create hydrophilic transmembrane pores. (c) G_9 (orange) deforms the membrane and inserts itself into a pocket. In all three systems, the polar heads of DOPG and DOPC are shown in green and red respectively, and the hydrophobic tails of the lipids in gray.

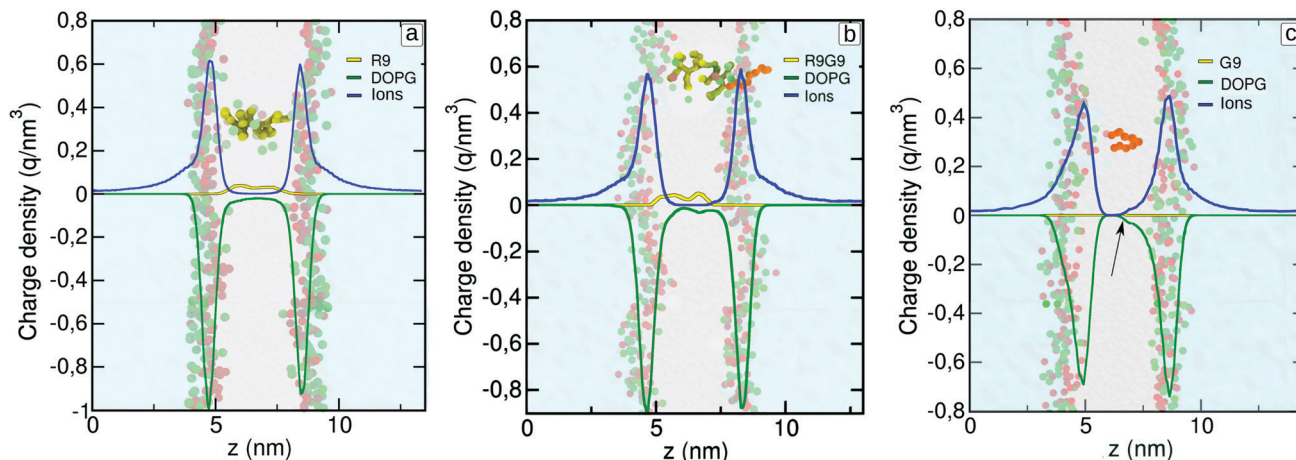


Fig. 4 Charge density profiles along the z -direction when the peptides are placed at the center of a DOPC–DOPG 1 : 1 bilayer. Each plot features three curves, the charge densities of DOPG (green), ions (blue), and the peptides (a) R_9 , (b) R_9G_9 , and (c) G_9 (all in yellow). At the back of each plot, there is a simulation snapshot depicting the location of the peptide (R_9 in yellow and G_9 in orange) in the bilayer. The head-groups of the lipids are shown in green (DOPG) and red (DOPC).

density of DOPG head-groups indicates a pronounced local dip on the membrane surface, with no continuity between leaflets. The dip is marked by the black arrow.

3.2 The negative surface charge enhances the CPP-effect of R_9

In order to examine the effect of electro-adsorption on translocation rates, we systematically varied the concentration of anionic lipid (DOPG) from 50 to 0%. Fig. 5 shows the insertion free-energy profiles for R_9 . In the case of the neutral bilayer (0% PG, blue curve in Fig. 5) the profile does not show an adsorption well near the water/lipid interface. Conversely, as the concentration of PG increases a clear minimum develops, whose depth approaches saturation at $\sim 50\%$ DOPG (see Table 1).

In living cells, CPP adsorption has been attributed to several anionic species commonly found on cell surfaces such as glycosaminoglycans, heparan sulfate and anionic phospholipids. Moreover, in lipid vesicles it has been documented that the incorporation of

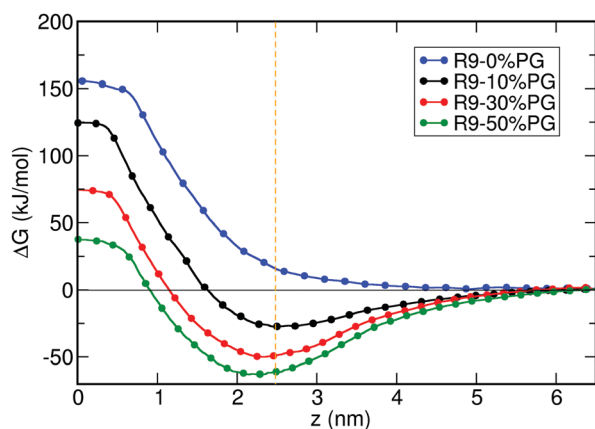


Fig. 5 Free-energy profiles for the insertion of R_9 in a DOPC/DOPG bilayer, bearing increasing percentages of DOPG: 0% (blue), 10% (black), 30% (red) and 50% (green). The vertical line indicates the average position of the membrane surface.

Table 1 Free-energy differences extracted from the profiles of Fig. 5 and 6. They refer to the processes of adsorption ($\Delta G_{z_{\min}}$), insertion ($\Delta G_{z=0}$) and activation ($\Delta G_{z_{\text{center}}-z_{\min}}$), of R_9 and R_9G_9 , in DOPC–DOPG lipid bilayers

%PG	R_9			R_9G_9		
	ΔG_{ins}	ΔG_{act}	ΔG_{ads}	ΔG_{ins}	ΔG_{act}	ΔG_{ads}
0	144 ± 4	144 ± 4	17 ± 3	176 ± 4	176 ± 4	17 ± 4
30	80 ± 4	130 ± 5	-50 ± 4	66 ± 4	116 ± 4	-50 ± 4
50	37 ± 3	98 ± 4	-61 ± 4	66 ± 4	129 ± 4	-63 ± 3

anionic lipids promotes the translocation of pArg.⁵¹ So far, the main hypothesis supporting the existence of an adsorption well for CPPs are, (a) the electrostatic interaction between the polycationic charge of the CPP and the anionic charges on the membrane; and (b) specific interactions between the guanidinium group of arginine and the phosphate, carboxylate, and sulfate groups of the phospholipids; *i.e.* hydrogen bonding. Although this second interaction is not taken into account by our coarse-grain model, it is also much weaker than the coulombic forces that drive electro-adsorption.

According to the model presented in Fig. 1, a decrease in ΔG_{ads} , ΔG_{act} , or both, reduce the value of ΔG_{ins} and enhance the translocation rate. At the first sight, the free energy curves of Fig. 5 show that the progressive increase in DOPG concentration is in lockstep with a decrease in ΔG_{ads} and ΔG_{act} . However, these variables do not vary proportionally. ΔG_{ins} is reduced by a factor of 4 when going from the neutral to the 50% PG bilayer, leading to a 18-orders of magnitude increase in the translocation rate. Since ΔG_{act} only decreases by a factor of 1.5, the decrease in ΔG_{ins} is mostly due to the drop in ΔG_{ads} induced by the anionic charges on the membrane (see Table 1).

It should also be noted from Fig. 5 that, as the negative charge increases, the position of the minimum shifts towards the center of the membrane ($z = 0$). This means that the electrostatic attraction between the membrane and R_9 pulls the peptide deeper into the membrane as the concentration of PG increases.

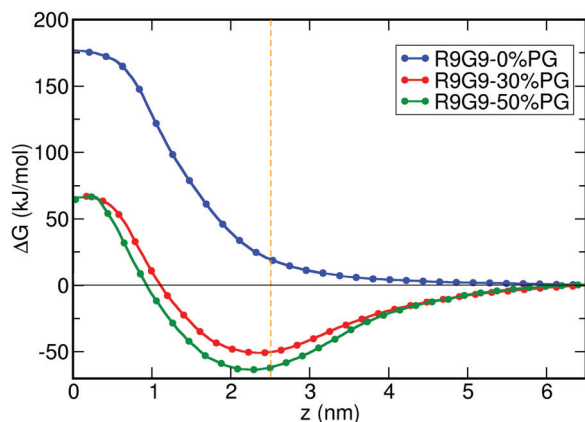


Fig. 6 Free-energy profiles for the insertion process of the R_9G_9 complex in a DOPC/DOPG bilayer bearing increasing concentration of anionic lipids: 0% (blue), 30% (red) and 50% (green) of DOPG. The vertical line indicates the average position of the membrane surface.

In the previous section, we showed that R_9 accelerates the translocation of the neutral cargo G_9 , as $\Delta G_{\text{act}}^{R_9G_9}$ was significantly lower than $\Delta G_{\text{act}}^{G_9}$. Additionally, we have shown that a negative surface charge favors the process of insertion of the CPP. Motivated by these results, we decided to evaluate the effect of the surface charge on the energy costs to transport the R_9G_9 complex across the bilayer.

Fig. 6 shows the free-energy profiles for R_9G_9 . In comparison with R_9 , there is a similar trend in ΔG_{ads} : increasing the concentration of DOPG from 0 to 30% yields an adsorption minimum that gets slightly deeper at 50% PG. Likewise, there is a subtle shift in the position of the minimum towards the mid-plane of the membrane. At the same time, the insertion energy of the CPP-cargo complex, $\Delta G_{\text{ins}}^{R_9G_9}$, drops significantly when adding 30% of anionic lipid, but it changes no further when going to 50% DOPG. This saturation effect stems from the fact that the slight drop in adsorption energy, when going from 30 to 50% PG, is compensated by a concomitant rise in activation energy. The latter could be ascribed to the absence of electrostatic interactions between the cargo and the rim of the pore, at variance with a cargo-free R_9 . As shown in Fig. 3b, the R_9G_9 complex nucleates a hydrophilic pore that becomes more anionic as the DOPG concentration rises.³² This condition is unfavorable for a neutral cargo like G_9 . In other words, the electroneutrality of G_9 could explain the slight increase in $\Delta G_{\text{act}}^{R_9G_9}$ when increasing the concentration of anionic lipid.

All in all, we have shown that electrostatic interactions provide a strong driving force for the translocation of both the cargo-free R_9 and the R_9G_9 complex. However, increasing the concentration of anionic lipids above 30% does not seem to enhance the CPP-effect of R_9 , at least for our simple neutral cargo.

3.3 Membrane ionized fatty acids facilitate the permeation of R_9

Experimental evidences suggest that fatty acids, species that occur naturally in cell membranes, could play a key role in the cellular intake of cell-penetrating peptides. Tentatively, this has been attributed to a combination of molecular properties, such

Table 2 Free-energy differences for the processes of adsorption ($\Delta G_{z_{\text{min}}}$), insertion ($\Delta G_{z=0}$) and activation (ΔG_{act}), of R_9 and R_9G_9 in bilayers made of: DOPC/PAH 75 : 25 (PAH: palmitic acid), DOPC/PA- 75 : 25 (PA-: palmitate), and DOPC/DOPG 70 : 30 bilayer (referenced as PG in columns four and six)

ΔG	R_9 /PAH	R_9 /PA-	R_9 /PG	R_9G_9 /PA-	R_9G_9 /PG
ΔG_{ins}	183 ± 4	30 ± 4	80 ± 5	21 ± 5	65 ± 6
ΔG_{ads}	19 ± 4	-47 ± 5	-50 ± 4	-47 ± 4	-50 ± 4
ΔG_{act}	183 ± 4	77 ± 5	130 ± 5	68 ± 5	115 ± 6

as small areas per molecule, short hydrocarbon tails, and the relatively large acidity constants of fatty acids that make their protonation state sensitive to the local pH.^{33,37}

In order to evaluate the potential impact of fatty acids on the transport mechanism of CPPs, we put together three systems with the following membrane compositions: (a) DOPC/PAH 75 : 25 (PAH: protonated palmitic acid), (b) DOPC/PA- 75 : 25 (PA-: ionized palmitic acid), and (c) DOPC/DOPG 70 : 30. The composition of system (b) was adjusted so that it yielded the same surface charge density as system (c). This allowed to assess the effect of the lipid type on the insertion of the peptides. Table 2 compares the associated free-energy costs for the insertion of R_9 and R_9G_9 . For the neutral DOPC/PAH membrane, the positive value of ΔG_{ads} for R_9 results from the lack of electrostatic attraction between the peptide and the membrane. The CPP also shows a very high insertion energy, of $\sim 180 \text{ kJ mol}^{-1}$. Deprotonation of the fatty acids leads to the spontaneous adsorption of the CPP, with a binding energy of $\Delta G_{\text{ads}} -47 \text{ kJ mol}^{-1}$, and a significant reduction in insertion energy ($\Delta G_{\text{ins}} \sim 153 \text{ kJ mol}^{-1}$). The clearly contrasting effects of PAH and PA- highlight again the relevance of electro-adsorption. However, when comparing the DOPC/PA- and DOPC/DOPG membranes bearing equivalent surface charges, we find similar adsorption energies but significant differences in the cost of peptide insertion. Our estimate, based on eqn (3), is that replacing DOPG by PA- increases the translocation rate of R_9 by 8 orders of magnitude.

Fig. 7 compares charge density profiles when R_9 is placed at the center of the DOPC-DOPG 70:30 bilayer (dashed line) or the DOPC/PA- 75:25 bilayer (full lines). When the CPP is restrained to the centre of the membrane, the local concentration of negative charge near the peptide is slightly higher when the membrane contains PA- (referenced as R-COO in Fig. 7). In other words, the fatty acid colocalises better with R_9 at the center of the bilayer, compensating its positive charge more effectively than DOPG.

The values reported in Table 2 also show that PA- favors the passage of the CPP-cargo complex over DOPG. When comparing the values of $\Delta G_{\text{ins}}^{R_9G_9}$ between DOPC/PA- and DOPC/DOPG membranes, eqn (3) yields an estimated translocation rate 7 orders of magnitude larger for the palmitate-containing membrane. Other things equal, this result illustrates how the size and shape of the lipids modulate the energetics of CPPs transport.

At the light of the adaptive translocation mechanism proposed by Rothbard *et al.*,⁵² we hypothesize that the catalytic effect of PA- is due to the greater configurational freedom introduced by single-tailed fatty acids over phospholipids. The packing freedom of

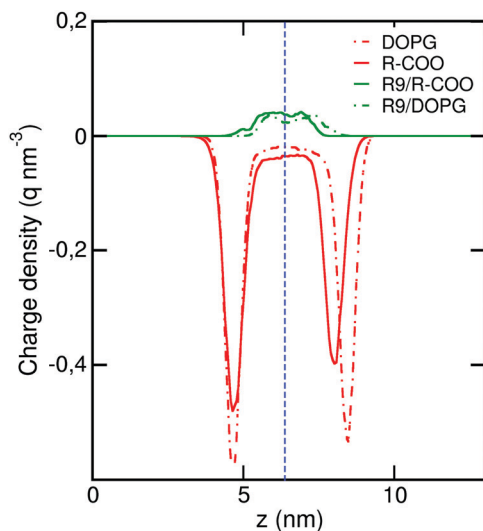


Fig. 7 Charge density profiles extracted from Umbrella sampling simulations where R_9 is restrained at the center of a DOPC/DOPG 70 : 30 bilayer (dash lines), or in a DOPC/PA 75 : 25 bilayer (full lines). The red curves show the charge density associated to charged lipids (DOPG or R-COO), while the green curves represent the charge density provided by R_9 .

PA- facilitates not only the screening of the CPPs' charges, but may also alleviate the mechanical tension produced by the nucleation of the transmembrane pore. In other words, the smaller mean molecular area of fatty acids would allow the formation of a more stable R_9 -PA- complex as the peptide diffuses across the membrane.^{33,53}

3.4 The size of the cargo modulates the CPP-effect of R_9

The bibliographic record shows that CPPs have been successfully used in combination with a large variety of cargoes such as liposomes,^{54,55} quantum dots,⁷ peptides,³ proteins,⁴ metallic nanoparticles,⁵⁶ RNA,^{5,6} and small fluorophores.^{8–10} Simple intuition tells that the chemical nature and elemental physical properties of the cargo, such as size, shape, and electric charge, are expected to influence the efficiency of the CPP-effect. So, in order to explore to what extent the size of the cargo modulates the translocation rate of the CPP-cargo complex, we computed insertion free-energy profiles for a linear peptide made of 31 glycine residues, G_{31} , and the corresponding R_9G_{31} complex. Both sequences were considered to have random coil structure in solution. The membrane was made of DOPC–DOPG 70 : 30. Table 3 collects the values of ΔG .

By comparing $\Delta G_{\text{ads}}^{G_{31}}$ and $\Delta G_{\text{ads}}^{R_9G_{31}}$, it is clear that a single R_9 molecule facilitates the binding of G_{31} to the membrane surface. However, a single R_9 sequence is not enough to promote the translocation of the complex across the membrane. In fact, the translocation rate of R_9G_{31} is about 2000-times smaller than that of the bare cargo. The data reported in Table 3 also show that the CPP efficiency of R_9 is greatly affected by the size of the cargo: a threefold increase in the size of the cargo tripled both $\Delta G_{\text{ins}}^{R_9G_{31}}$ and $\Delta G_{\text{act}}^{R_9G_{31}}$. At the light of the results presented in this paper, a potential solution to the transport of G_{31} , or of any large cargo for that matter, would be to increase the number of

Table 3 Free-energy differences for the processes of adsorption ($\Delta G_{z_{\text{min}}}$), insertion ($\Delta G_{z=0}$) and activation ($\Delta G_{z_{\text{center}}-z_{\text{min}}}$), of G_{31} and R_9G_{31} in a DOPC/DOPG 70 : 30 bilayer

ΔG (kJ mol ⁻¹)	G_{31}	R_9G_{31}	R_9G_9
ΔG_{ins}	200 ± 7	220 ± 6	65 ± 6
ΔG_{ads}	0 ± 1	-77 ± 3	-50 ± 4
ΔG_{act}	200 ± 5	307 ± 5	115 ± 6

CPP molecules linked to the cargo. That would certainly lower $\Delta G_{\text{ads}}^{R_9G_{31}}$ and may shift down the whole free-energy curve so that $\Delta G_{\text{ins}}^{R_9G_{31}} < \Delta G_{\text{ins}}^{G_{31}}$.

4 Conclusions

The CPP-effect makes reference to the process by which the membrane translocation rate of a cargo is enhanced by chemical functionalization with cell-penetrating peptides. In the present work we combined a simple kinetic model with coarse-grained molecular dynamics simulations to explore the energetic basis of the CPP-effect. We selected two polyglycines as model hydrophilic cargoes, G_9 and G_{31} , and nona-arginine R_9 , as a prototypical CPP. First, our results indicated that G_9 is unable to cross a lipid bilayer at least conjugated with R_9 . The CPP-effect was caused by the strong binding of the CPP-cargo complex, R_9G_9 , to the surface of the membrane, and a lower translocation barrier for the complex as compared to the naked cargo. All CPP bear a large electrical charge. Our simulations indicated that electrostatic interactions impact strongly both on the adsorption and activation free-energy of the CPP-cargo complex. In turn, these thermodynamic parameters determine the translocation rate and are sensitive to environmental conditions.

We assessed the role of the surface charge of the membrane by computing the peptides' insertion free-energy cost in membranes made of DOPC and varying amounts of the anionic lipid DOPG. It was observed that the negative charge density of the membrane modulates the CPP-effect by promoting the adsorption and even the insertion of both the CPP and the CPP-cargo complex. Moreover, the shape and size of a minor fraction of the lipids was able to enhance the CPP-effect. This was demonstrated by replacing DOPG, at constant surface charge density, by deprotonated palmitic acid, PA-. It was found that the fatty acid accelerates the membrane translocation of both R_9 and R_9G_9 . The catalytic role of PA- was attributed to its greater packing freedom as compared with DOPG. As a single-chain fatty acid, PA- seems to form a more stable R_9 -PA- coordination complex as the peptide diffuses across the membrane.

Finally, we presented evidence indicating that the size of the cargo matters. While G_9 crossed the membrane more readily when linked to a single R_9 molecule, the same did not happen for G_{31} . For these particular systems, tripling the size of the cargo shut out the CPP-effect. This observation rose the important question of how many CPP molecules are needed to transport a cargo of a given size and shape. The answer to that question may

help design more effective CPP–cargo complexes and will be the object of a future study.

Conflicts of interest

The authors declare no conflicts of interest.

Acknowledgements

The authors thank CONICET, SECTyP-UNCUYO and FONCyT-ANPCyT (PICT 2012-0344, PICT-2012-2759, PICT-2015-1835) for research funding. We are also grateful to the EU Commission Marie Curie RISE “ENACT” Programme (643998), and SNCAD-MinCyT for computer time allocation in the clusters Mendieta (CCAD-UNC) and Toko (UNCUYO). N. W., L. S. M. and M. G. D. P. are CONICET researchers, and M. A. V. is a PhD fellow from CONICET.

References

- E. Koren and V. P. Torchilin, *Trends Mol. Med.*, 2012, **18**, 385–393.
- E. Vives, *J. Controlled Release*, 2005, **109**, 77–85.
- D. Kim, I.-H. Lee, S. Kim, M. Choi, H. Kim, S. Ahn, P. E. Saw, H. Jeon, Y. Lee and S. Jon, *Cancer Res.*, 2014, **74**, 2144–2151.
- A. Bolhassani, B. S. Jafarzade and G. Mardani, *Peptides*, 2017, **87**, 50–63.
- S. Park, E. J. Jeong, J. Lee, T. Rhim, S. K. Lee and K. Y. Lee, *Carbohydr. Polym.*, 2013, **92**, 57–62.
- J. R. Kanwar, G. Mahidhara and R. K. Kanwar, *Drug Discovery Today*, 2011, **16**, 188–202.
- B. R. Liu, Y. Wern Huang, J. G. Winiarz, H.-J. Chiang and H.-J. Lee, *Biomaterials*, 2011, **32**, 3520–3537.
- E. N. Savariar, C. N. Felsen, N. Nashi, T. Jiang, L. G. Ellies, P. Steinbach, R. Y. Tsien and Q. T. Nguyen, *Cancer Res.*, 2013, **73**, 855–864.
- G. Candan, H. Michiue, S. Ishikawa, A. Fujimura, K. Hayashi, A. Uneda, A. Mori, I. Ohmori, T. Ichi Nishiki, H. Matsui and K. Tomizawa, *Biomaterials*, 2012, **33**, 6468–6475.
- T. Takeuchi, M. Kosuge, A. Tadokoro, Y. Sugiura, M. Nishi, M. Kawata, N. Sakai, S. Matile and S. Futaki, *ACS Chem. Biol.*, 2006, **1**, 299–303.
- S. Deshayes, M. C. Morris, G. Divita and F. Heitz, *Cell. Mol. Life Sci.*, 2005, **62**, 1839–1849.
- H. Mitsui, T. Inozume, R. Kitamura, N. Shibagaki and S. Shimada, *J. Invest. Dermatol.*, 2006, **126**, 1804–1812.
- O. Veis, F. M. Kievit, H. Mok, J. Ayesh, C. Clark, C. Fang, M. Leung, H. Arami, J. O. Park and M. Zhang, *Biomaterials*, 2011, **32**, 5717–5725.
- S. W. Jones, R. Christison, K. Bundell, C. J. Joyce, S. M. V. Brockbank, P. Newham and M. A. Lindsay, *Br. J. Pharmacol.*, 2005, **145**, 1093–1102.
- P. E. G. Thören, D. Persson, E. K. Esbjörner, M. Goksor, P. Lincoln and B. Nordén, *Biochemistry*, 2004, **43**, 3471–3489.
- S. El-Andaloussi, T. Holm and U. Längel, *Curr. Pharm. Des.*, 2005, **11**, 3597–3611.
- S. M. Farkhani, A. Valizadeh, H. Karami, S. Mohammadi, N. Sohrabi and F. Badrzadeh, *Peptides*, 2014, **57**, 78–94.
- M. Di Pisa, G. Chassaing and J.-M. Swiecicki, *Biochemistry*, 2015, **54**, 194–207.
- W. B. Kauffman, T. Fuselier, J. He and W. C. Wimley, *Trends Biochem. Sci.*, 2015, **40**, 749–764.
- Y. Pouny, D. Rapaport, A. Mor, P. Nicolas and Y. Shai, *Biochemistry*, 1992, **31**, 12416–12423.
- D. Derossi, A. H. Joliot, G. Chassaing and A. Prochiantz, *J. Biol. Chem.*, 1994, **269**, 10444–10450.
- K. Matsuzaki, S. Yoneyama, O. Murase and K. Miyajima, *Biochemistry*, 1996, **35**, 8450–8456.
- F. Madani, S. Lindberg, L. Längel and S. Futaki, *J. Biophys.*, 2011, **2011**, 1–10.
- D. Sun, J. Forsman, M. Lund and C. E. Woodward, *Phys. Chem. Chem. Phys.*, 2014, **16**, 20785–20795.
- J. Ye, E. Liu, Z. Yu, X. Pei, S. Chen, P. Zhang, M.-C. Shin, J. Gong, H. He and V. C. Yang, *Int. J. Mol. Sci.*, 2016, **17**, 1892.
- Y. Hu and S. Patel, *J. Membr. Biol.*, 2015, **248**, 505–515.
- Y. Hu and S. Patel, *Soft Matter*, 2016, **12**, 6716–6727.
- K. Huang and A. E. García, *Biophys. J.*, 2013, **104**, 412–420.
- H. Herce, A. Garcia, J. Litt, R. Kane, P. Martin, N. Enrique, A. Rebolledo and V. Milesi, *Biophys. J.*, 2008, **97**, 1917–1925.
- M. A. Via, J. Klug, N. Wilke, L. S. Mayorga and M. G. Del Pópolo, *Phys. Chem. Chem. Phys.*, 2018, **20**, 5180–5189.
- A. Komin, L. Russell, K. Hristova and P. Searson, *Adv. Drug Delivery Rev.*, 2017, **110–111**, 52–64.
- P. G. Ramírez, M. G. D. Pópolo, J. A. Vila, I. Szleifer and G. S. Longo, *J. Colloid Interface Sci.*, 2019, **552**, 701–711.
- M. A. Via, M. G. Del Pópolo and N. Wilke, *Langmuir*, 2018, **34**, 3102–3111.
- G. Grasso, S. Muscat, M. Rebella, U. Morbiducci, A. Audenino, A. Danani and M. A. Deriu, *J. Biomech.*, 2018, **73**, 137–144.
- J. Lin and A. Alexander-Katz, *ACS Nano*, 2013, **7**, 10799–10808.
- Z. Li, H. Ding and Y. Ma, *Soft Matter*, 2013, **9**, 1281–1286.
- H. D. Herce, A. E. García and M. C. Cardoso, *J. Am. Chem. Soc.*, 2014, **136**, 17459–17467.
- M. J. Abraham, T. Murtola, R. Schulz, S. Páll, J. C. Smith, B. Hess and E. Lindahl, *SoftwareX*, 2015, **1–2**, 19–25.
- S. J. Marrink, H. J. Risselada, S. Yefimov, D. P. Tieleman and A. H. de Vries, *J. Phys. Chem. B*, 2007, **111**, 7812–7824.
- T. A. Wassenaar, H. I. Ingólfsson, R. A. Böckmann, D. P. Tieleman and S. J. Marrink, *J. Chem. Theory Comput.*, 2015, **11**, 2144–2155.
- G. Torrie and J. Valleau, *J. Comput. Phys.*, 1977, **23**, 187–199.
- B. Roux, *Comput. Phys. Commun.*, 1995, **91**, 275–282.
- K. Dill and S. Bromberg, *Molecular Driving Forces*, Garland Science, 2010.
- D. Mitchell, L. Steinman, D. Kim, C. Fathman and J. Rothbard, *J. Pept. Res.*, 2000, **56**, 318–325.
- Y. Su, T. Doherty, A. J. Waring, P. Ruchala and M. Hong, *Biochemistry*, 2009, **48**(21), 4587–4595.
- H. L. Åmand, H. A. Rydberg, L. H. Fornander, P. Lincoln, B. Nordén and E. K. Esbjörner, *Biochim. Biophys. Acta, Biomembr.*, 2012, **1818**, 2669–2678.

- 47 P. A. Wender, D. J. Mitchell, K. Pattabiraman, E. T. Pelkey, L. Steinman and J. B. Rothbard, *Proc. Natl. Acad. Sci. U. S. A.*, 2000, **97**, 13003–13008.
- 48 Y. Takechi, H. Yoshii, M. Tanaka, T. Kawakami, S. Aimoto and H. Saito, *Langmuir*, 2011, **27**, 7099–7107.
- 49 Y. Hu, X. Liu, S. K. Sinha and S. Patel, *J. Phys. Chem. B*, 2014, **118**, 2670–2682.
- 50 M. Crosio, M. Via, C. Cámara, A. Mangiarotti, M. Del Pópulo and N. Wilke, *Biomolecules*, 2019, **9**, 625.
- 51 A. D. Robison, S. Sun, M. F. Poyton, G. A. Johnson, J.-P. Pellois, P. Jungwirth, M. Vazdar and P. S. Cremer, *J. Phys. Chem. B*, 2016, **120**, 9287–9296.
- 52 J. B. Rothbard, T. C. Jessop and P. A. Wender, *Adv. Drug Delivery Rev.*, 2005, **57**, 495–504.
- 53 J.-M. Swiecicki, A. Bartsch, J. Tailhades, M. Di Pisa, B. Heller, G. Chassaing, C. Mansuy, F. Burlina and S. Lavielle, *Chem-BioChem*, 2014, **15**, 884–891.
- 54 Y. Liu, R. Ran, J. Chen, Q. Kuang, J. Tang, L. Mei, Q. Zhang, H. Gao, Z. Zhang and Q. He, *Biomaterials*, 2014, **35**, 4835–4847.
- 55 S. Biswas, P. P. Deshpande, F. Perche, N. S. Dodwadkar, S. D. Sane and V. P. Torchilin, *Cancer Lett.*, 2013, **335**, 191–200.
- 56 S. M. Farkhani, A. A. Fard, P. Zakeri-Milani, J. S. Mojarrad and H. Valizadeh, *Artif. Cells, Nanomed., Biotechnol.*, 2017, **45**, 1029–1035.